Correlation and orbit determination of space objects based on sparse optical data

A. Milani,[1]* G. Tommei,[1]* D. Farnocchia,[1]* A. Rossi,[2]* T. Schildknecht[3]*
and R. Jehn[4]*

[1]*Dipartimento di Matematica, Università di Pisa, 56127 Pisa, Italy*
[2]*IFAC-CNR, Firenze & ISTI-CNR, 56124 Pisa, Italy*
[3]*Astronomical Institute, University of Bern, 3012 Bern, Switzerland*
[4]*ESA-ESOC, 64293 Darmstadt, Germany*

ABSTRACT

While building up a catalogue of Earth-orbiting objects, the available optical observations are typically sparse. In this case, no orbit determination is possible without previous correlation of observations obtained at different times. This correlation step is the most computationally intensive, and becomes more and more difficult as the number of objects to be discovered increases. In this paper, we tested two different algorithms, and the related prototype software, recently developed to solve the correlation problem for objects in geostationary orbit (GEO). The algorithms allow the accurate orbit determination by full least-squares solutions with all six orbital elements. The presence of a significant subpopulation of high area-to-mass ratio objects in the GEO region, strongly affected by non-gravitational perturbations, required to solve also for dynamical parameters describing these effects, that is to fit between six and eight free parameters for each orbit.

The validation was based upon a set of real data, acquired from the European Space Agency (ESA) Space Debris Telescope (ESASDT) at the Teide Observatory (Canary Islands). We proved that it is possible to assemble a set of sparse observations into a set of objects with orbits. This would allow a survey strategy covering the region of interest in the sky just once per night. As a result, it would be possible to significantly reduce the requirements for a future telescope network, with respect to what would have been required with the previously known algorithms for correlation and orbit determination.

Key words: methods: analytical – methods: data analysis – catalogues – astrometry – celestial mechanics.

1 INTRODUCTION

More than 16 000 objects with diameter larger than approximately 10 cm are orbiting the Earth. Only about 6 per cent of them are operational satellites. All the rest is composed by different types of space debris that now represent a serious hazard to the safe exploitation of the circumterrestrial space.

Most of the catalogued objects reside in the low Earth orbit (LEO) regime, i.e. they spend most of their life below 2000 km of altitude. This is the region of space with the highest spatial density of objects and where all the known collisions took place. None the less, another region of space hosts a large number of spacecraft that are crucial for our everyday life. It is the geosynchronous region, at an altitude of about 36 000 km (e.g. Rossi 2011). This paper deals specifically with objects orbiting in this region.

The growing risk posed by the overcrowding of the space calls for a number of measures capable in particular of minimizing the risk of collision between operational spacecraft and space debris. This requires the accurate knowledge of the orbit of both the objects. Currently, the major effort in tracking and cataloguing the space debris population is performed by the United States Strategic Command (USSTRATCOM) using a large network of radar and optical sensors located worldwide. The majority of the larger objects are catalogued by the USSTRATCOM in the Two-Line Element (TLE) catalogue. In this catalogue, about 16 000 objects are listed along with their current orbital parameters. The limiting size of the objects included in the catalogue (due to limitations in sensors power and in observation and data processing procedures) is about 5–10 cm below a few thousands km of altitude and about 0.5–1 m in higher orbits up to the geostationary orbit (GEO) ones.

*E-mail: milani@dm.unipi.it (AM); tommei@dm.unipi.it (GT); farnocchia@mail.dm.unipi.it (DF); A.Rossi@ifac.cnr.it (AR); thomas.schildknecht@aiub.unibe.ch (TS); Ruediger.Jehn@esa.int (RJ)

In particular, currently about 1000 objects, with diameter larger than about 1 m, are classified as geosynchronous objects (mean motion between 0.9 and 1.1 and eccentricity not greater than 0.2) in the TLE catalogue (Choc & Jehn 2010). On the other hand, dedicated optical campaigns from the ESA Space Debris Telescope (ESASDT) (a 1-m telescope located on the Teide volcano, in the Canary Islands), and from other similar American or Russian sensors, revealed a large number of so-called *uncorrelated objects*, i.e. objects not present in the TLE catalogue. Most of these are probably the result of a still undetermined number of explosions occurred to spacecraft and upper stages. Dedicated optical observation campaigns were performed to characterize the environment in this orbital region (e.g. Schildknecht et al. 2005) for objects down to a few tens of cm.

Moreover, in recent years, a peculiar population of objects having mean motion around 1 and high eccentricity (as high as 0.55) was detected by the ESASDT (Schildknecht et al. 2004). It was shown that these are objects with very high area-to-mass ratio (A/M) (ranging from 1 up to 30 m² kg⁻¹) whose dynamics is therefore strongly perturbed by the solar radiation pressure that significantly affects their eccentricity (and also their inclination) with small effects on the total energy of the orbit and, therefore, on the semimajor axis or mean motion (Liou & Weaver 2005). Most probably these objects are remnants of thermal blankets or multilayer insulation either detached from aging spacecraft or ejected by explosive fragmentations of old spacecraft. It is worth noting that, from an observational point of view, these objects represent a particularly demanding task. Their dynamics is extremely difficult to model, due to the large influence of the solar radiation pressure, further complicated by the unknown and rapidly changing physical properties of the objects. This translates in a comparable difficulty in the determination of their orbits (Musci, Schildknecht & Ploner 2010). In Section 3, the algorithm used for the orbit determination of high A/M objects will be described.

Until recently, most of the dedicated observations have not been devoted to cataloguing purposes and have not led to a full orbit determination. The information obtained in the surveys made since 1999 are mainly statistical since no attempt has been made to catalogue the objects. This means that some objects may have been observed multiple times. From a probabilistic analysis, in Jehn et al. (2006) it is pointed out that the population of debris, brighter than visual magnitude 18.5, inferred from the ESASDT, may indeed suffer from multiple observations. This might have led to the overestimation of this particular population by a factor of about 5.

The procedures described in this paper were devised to solve this problem and to provide effective algorithms for the building of a European catalogue, analogous to the TLE one, foreseen in the framework of the European Space Situation Awareness (SSA) initiative. The SSA intends to provide Europe with an autonomous capacity to monitor the circumterrestrial space allowing a safe exploitation of this resource.

In Sections 2 and 3, we briefly recall the main features of the algorithms developed by our group in the last years for the orbit determination of space objects. Then the data set used to validate the algorithms is presented. And, finally, the results obtained are discussed.

2 ALGORITHMS

Given two or more sets of observations, the main problem is how to identify which separate sets of data belong to the same physical object (the so-called *correlation* problem). Thus, the orbit determi-

nation problem needs to be solved in two stages: first, different sets of observations need to be correlated; then an orbit can be determined. This combined procedure is called *linkage* in the literature (see Milani 1999).

Two different linkage methods were developed in the last few years. The algorithms are fully described in Tommei, Milani & Rossi (2007), Farnocchia et al. (2010), Gronchi, Dimare & Milani (2010) and Milani & Gronchi (2010). In this section, for ease of reading, we will briefly recall the main features of these algorithms, directing the reader to the above-cited papers for the full mathematical treatment.

2.1 Observations and attributables

To understand the results presented in the following sections, some nomenclature and definitions have to be introduced.

The batches of observations which can be immediately assigned to a single object give us a set of data that can be summarized in an *attributable*, that is a four-dimensional vector. To compute a full orbit, formed by six parameters, we need to know two further quantities.

Let $(\rho, \alpha, \delta) \in \mathbb{R}^+ \times [0, 2\pi) \times (-\pi/2, \pi/2)$ be topocentric spherical coordinates for the position of an Earth satellite. The angular coordinates (α, δ) are defined by a topocentric reference system that can be arbitrarily selected. Usually, in the applications, α is the right ascension and δ the declination with respect to an equatorial reference system (e.g. J2000). The values of range ρ and range rate $\dot{\rho}$ are not measured.

We shall call *optical attributable* a vector

$$\boldsymbol{A}_{\text{opt}} = (\alpha, \delta, \dot{\alpha}, \dot{\delta}) \in [0, 2\pi) \times (\pi/2, \pi/2) \times \mathbb{R}^2 \,,$$

representing the angular position and velocity of the body at a time t in the selected reference frame (for the definition of the radar attributable, see Tommei et al. 2007).

Given the attributable $\boldsymbol{A}$, to define an orbit the values of two unknowns quantities (e.g. ρ and $\dot{\rho}$) need to be found at the same instance in time as the attributable. These two quantities, together with $\boldsymbol{A}$, give us a set of *attributable orbital elements*,

$$\boldsymbol{X} = [\alpha, \delta, \dot{\alpha}, \dot{\delta}, \rho, \dot{\rho}],$$

at a time $\bar{t}$, computed from t taking into account the light-time correction: $\bar{t} = t - \rho/c$ (c being the velocity of light). Of course, the information on the observer station must be available.

Starting from an attributable, we would like to extract sufficient information in order to compute full preliminary orbits.

2.2 Virtual debris algorithm

The first algorithm developed is called the virtual debris algorithm and makes use of the so-called *admissible region*.

The admissible region replaces the conventional confidence region as defined in the classical orbit determination procedure. The main requirement is that the geocentric energy of the object is negative, so that the object is a satellite of the Earth.

Given the geocentric position $\boldsymbol{r}$ of the debris, the geocentric position $\boldsymbol{q}$ of the observer, and the topocentric position $\boldsymbol{\rho}$ of the debris, we have $\boldsymbol{r} = \boldsymbol{\rho} + \boldsymbol{q}$. The energy (per unit mass) is given by

$$\mathcal{E}(\rho, \dot{\rho}) = \frac{1}{2} ||\dot{\boldsymbol{r}}(\rho, \dot{\rho})||^2 - \frac{\mu}{||\boldsymbol{r}(\rho)||} \,, \tag{1}$$

where μ is the Earth's gravitational parameter. Then a definition of admissible region such that only satellites of the Earth are allowed
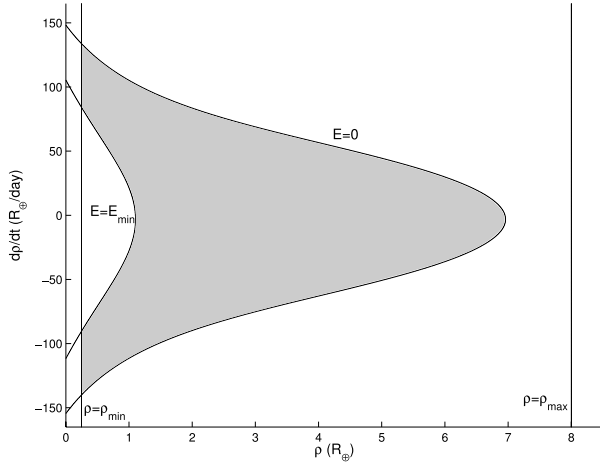
Figure 1. An example of admissible region in the $(\rho, \dot{\rho})$ plane. The region (painted in grey) is bounded by two level curves of the energy, $E = E_{\min}$ and 0, and by the two conditions on the topocentric distance ($\rho = \rho_{\min}$ and $\rho_{\max}$).

includes the condition

$$\mathcal{E}(\rho, \dot{\rho}) \leq 0. \tag{2}$$

This condition translates in a region of $(\rho, \dot{\rho})$ having at most two connected components (even if in a large number of numerical experiments with objects in the Earth orbit, we have not found examples with two connected components). The admissible region needs to be compact in order to have the possibility to sample it with a finite number of points; thus, a condition defining an inner boundary needs to be added. The choice for the inner boundary depends upon the specific orbit determination task: a simple method is to add constraints $\rho_{\min} \leq \rho \leq \rho_{\max}$ allowing us, e.g., to focus the search of identifications to one of the three classes – LEO, Medium Earth Orbit (MEO) and GEO. Another natural choice for the inner boundary is to take $\rho \geq h_{\mathrm{atm}}$, where h_{atm} is the thickness of a portion of the Earth atmosphere in which a satellite cannot remain in orbit for a significant time-span. As an alternative, it is possible to constrain the semimajor axis to be larger than $R_{\oplus} + h_{\mathrm{atm}} = r_{\min}$, where h_{atm} is the radius of the Earth atmosphere. The qualitative structure of the admissible region is shown in Fig. 1.

The shaded region of Fig. 1 can be further constrained and reduced excluding trajectories impacting the Earth in less than one revolution, which means to impose that the perigee is larger than a given value $r_{\min}$ (Maruskin, Scheeres & Alfriend 2009; Farnocchia et al. 2010).

Once the admissible region is defined it has to be discretized, sampling it to generate a swarm of *virtual debris*. This is done using the Delaunay triangulation (Milani et al. 2004). The idea is to generate a swarm of virtual debris X_i, corresponding to the nodes of the admissible region of one of the two attributables, let us say A_1. Then we compute, from each of the X_i, a prediction A_i for the epoch t_2, each with its covariance matrix Γ_{A_i}. Thus, for each virtual debris X_i we can compute an attribution penalty K_4^i (Milani et al. 2005; Milani & Gronchi 2010, chapter 8) and use the values as a criterion to select some of the virtual debris to proceed to the orbit computation.

Thus, the procedure is as follows. We select some maximum value $K_{\max}$ for the attribution penalty and if there are some nodes such that $K_4^i \leq K_{\max}$ we proceed to the correlation confirmation (see Section 2.4). If this is not the case, we can try with another method, such as the one described in Section 2.3.

2.3 Keplerian integrals method

An alternative method to produce preliminary orbits starting from two attributables A_1, A_2 of the same object at two epoch times t_1 and t_2 was proposed for the asteroid case in Gronchi et al. (2010) and is based on the two-body integrals. The method was implemented and adapted to the space debris case (Farnocchia et al. 2010). Once more the procedure is applicable to both optical and radar observations, but only the optical case will be recalled here. We assume that the orbit between t_1 and t_2 is well approximated by a Keplerian two-body orbit, with constant energy $\mathcal{E}$ and angular momentum vector $\boldsymbol{c}$:

$$\begin{cases} \mathcal{E}(t_1) - \mathcal{E}(t_2) = 0 \\ \boldsymbol{c}(t_1) - \boldsymbol{c}(t_2) = 0 \end{cases}. \tag{3}$$

Solving the system (3) requires a complex analytical and numerical procedure, involving algebraic equations. This is detailed in Gronchi et al. (2010) and Farnocchia et al. (2010) and it is not worth recalling here. Once the roots of the equation are obtained, given all the roots which could be real, we select the positive couples (ρ_1, ρ_2) and remove the spurious ones. If the number of remaining solutions is zero, the attributables cannot be correlated with this method, otherwise the selected couple represents the sought for solution.

Once a solution of equation (3) is computed, the values of attributable elements can be obtained for the epochs $\bar{t}_1$ and $\bar{t}_2$, and they can be converted into the usual Keplerian elements:

$$(a_j, e_j, I_j, \Omega_j, \omega_j, \ell_j), \; j = 1, 2,$$

where ℓ_j are the mean anomalies. The first four Keplerian elements $(a_j, e_j, I_j, \Omega_j)$ are functions of the two-body energy and angular momentum vectors $\mathcal{E}_j$, $\boldsymbol{c}_j$, and are the same for $j = 1, 2$. Thus, the result can be assembled in the eight-dimensional vector:

$$\boldsymbol{H} = (\boldsymbol{V}, \boldsymbol{\Phi}_1, \boldsymbol{\Phi}_2), \quad \boldsymbol{V} = (a, e, I, \Omega)$$
$$\boldsymbol{\Phi}_1 = (\omega_1, \ell_1), \; \boldsymbol{\Phi}_2 = (\omega_2, \ell_2). \tag{4}$$

There are compatibility conditions between $\boldsymbol{\Phi}_1$ and $\boldsymbol{\Phi}_2$ to be satisfied if the two attributables belong to the same object:

$$\omega_1 = \omega_2, \; \ell_1 = \ell_2 + n(\bar{t}_1 - \bar{t}_2), \tag{5}$$

where $n = n(a)$ is the mean motion. We cannot demand the exact equality in the formulae above, because of various error sources, including the uncertainty of the attributable, and the changes on the Keplerian integrals due to the perturbations with respect to the two-body model. Thus, we need a metric to measure in an objective way the residuals in the compatibility conditions. The two attributables A_1, A_2 have been computed from the observations by using a least-squares fit to the individual observations, thus 4×4 covariance matrices Γ_{A_1} and Γ_{A_2} are available; they can be used to form the block diagonal 8×8 covariance matrix for both attributables Γ_A. The Keplerian integral method allows us to compute explicitly the vector $\boldsymbol{H}$ of equation (4) and, by means of the implicit function theorem, its partial derivatives. Thus, it is possible by the standard covariance propagation formula (Milani & Gronchi 2010, section 5.5) to compute also Γ_H, the covariance of $\boldsymbol{H}$. With another transformation we can compute the average elements $\boldsymbol{\Phi}_0 = (\boldsymbol{\Phi}_1 + \boldsymbol{\Phi}_2)/2$ [as the best value for the angular elements at time $\bar{t}_0 = (\bar{t}_1 + \bar{t}_2)/2$] and the discrepancy $\Delta\boldsymbol{\Phi}$ in the compatibility conditions (equation 5). Finally, we can propagate the covariance also to this eight-dimensional vector:

$$\Gamma_A \Longrightarrow \Gamma_H \Longrightarrow \Gamma_{V, \boldsymbol{\Phi}_0, \Delta\boldsymbol{\Phi}}.$$

The above argument is a generalization of the one in Gronchi et al. (2010), where explicit computations are given for the optical attributables case.

In the 8×8 covariance matrix $\boldsymbol{\Gamma}_{V,\boldsymbol{\Phi}_0,\Delta\boldsymbol{\Phi}}$, the lower right 2×2 block is the marginal covariance matrix of $\Delta\boldsymbol{\Phi}$, from which we can compute the normal matrix and the χ^2:

$$\mathbf{C}_{\Delta\boldsymbol{\Phi}} = \boldsymbol{\Gamma}_{\Delta\boldsymbol{\Phi}}^{-1}, \quad \chi^2_{\Delta\boldsymbol{\Phi}} = \Delta\boldsymbol{\Phi} \cdot \mathbf{C}_{\Delta\boldsymbol{\Phi}} \, \Delta\boldsymbol{\Phi},$$

which can be used as control. This control checks whether the discrepancy in the compatibility conditions is consistent with the observation error. The correlation between the two attributables is considered possible only if $\chi^2_{\Delta\boldsymbol{\Phi}} \leq \chi^2_{\max}$.

The upper left 6×6 block is the covariance matrix of the preliminary orbit, that is of the orbital elements set $(V, \boldsymbol{\Phi}_0)$ (at epoch $\bar{t}_0$). Although this preliminary orbit is just a two-body solution, it has an uncertainty estimate, arising from the (supposedly known) statistical properties of the observational errors. This estimate neglects the influence of perturbations, such as the spherical harmonics of the Earth gravity field, the lunisolar differential attraction and the non-gravitational perturbations; nevertheless, if the time-span $\bar{t}_2 - \bar{t}_1$ is short, the covariance obtained above can be a useful approximation. Recently, the method was generalized, including the effect due to the non-spherical shape of the Earth (Farnocchia et al. 2010), thus allowing its application also to objects in LEO. On the other hand, since the present paper deals only with high Earth orbit data, where the effect of J_2 on the angular momentum of the objects is strongly reduced by the distance from the centre of the Earth, all the analysis presented in this paper was performed without the inclusion of the J_2 effect.

Note that there are some cases in which the Keplerian integrals method cannot be applied.

We have to avoid the condition $(\boldsymbol{q}_1 \times \hat{\boldsymbol{\rho}}_1) \times (\boldsymbol{q}_2 \times \hat{\boldsymbol{\rho}}_2) = 0$, where $\boldsymbol{q}_1$ and $\boldsymbol{q}_2$ are the observer geocentric positions at the instants t_1 and t_2. This can happen when

(i) $\boldsymbol{q}_1$ is parallel to $\hat{\boldsymbol{\rho}}_1$, i.e. the observation at time t_1 is done at the observer zenith,

(ii) $\boldsymbol{q}_2$ is parallel to $\hat{\boldsymbol{\rho}}_2$, i.e. the observation at time t_2 is done at the observer zenith and

(iii) $\boldsymbol{q}_1, \boldsymbol{q}_2, \hat{\boldsymbol{\rho}}_1$ and $\hat{\boldsymbol{\rho}}_2$ are coplanar. This case arises whenever a geostationary object is observed from the same station at the same hour of distinct nights.

As it is normal, the mathematical singularity is surrounded by a neighbourhood in which the method is possible for zero error (both zero observational error and zero rounding off in the computation), but is not applicable in practice due to the limited numerical accuracy, e.g. this method fails even for non-geostationary, nearly geosynchronous orbits with hours of observations over different nights differing by only a few minutes each night. Note that in an observing strategy optimized for the use of this method, this occurrence can be easily avoided.

2.4 Correlation confirmation

The multiple orbits obtained with both methods from Sections 2.2 and 2.3 are just preliminary orbits, solution of a two-body approximation (as in the classical methods of Laplace and Gauss). They have to be replaced by least-squares orbits, with a dynamical model including all the relevant perturbations.

Even after confirmation by least-squares fit, it might still be the case that some linkages with just two attributables can be *false*, that is the two attributables might belong to different objects. This is

confirmed by the tests with real data reported in Tommei et al. (2009) for the virtual debris method and in Milani et al. (2009) for the Keplerian integrals method. Thus, every linkage of two attributables needs to be confirmed by correlating a third attributable.

The process of looking for a third attributable which can also be correlated to the other two is called *attribution* (Milani 1999; Milani, Sansaturio & Chesley 2001). From the available two-attributable orbit with covariance, we predict the attributable $\boldsymbol{A}_P$ at the time t_3 of the third attributable, and compare with $\boldsymbol{A}_3$ computed from the third set of observations. Both $\boldsymbol{A}_P$ and $\boldsymbol{A}_3$ come with a covariance matrix; we can compute the χ^2 of the difference and use it as a test. For the attributions passing this test we proceed to the differential corrections. The procedure is recursive, that is we can use the three-attributable orbit to search for attribution of a fourth attributable, and so on. This generates a very large number of many-attributable orbits, but there are many duplications, corresponding to adding them in a different order.

A specific procedure, called *correlation management*, is used to remove duplicates (e.g. giving three tracklets, or attributables, A, B, C, $A = B = C$ and $A = C = B$) and inferior correlations (e.g. $A = B = C$ is superior to both $A = B$ and $C = D$, thus both are removed). The output catalogue after this process is called normalized. In the process, we may try to merge two correlations with some attributables in common, by computing a common orbit (Milani et al. 2005).

Due to the characteristics of the two methods briefly outlined in this section, it can be noted that the two algorithms have different ranges of application. The virtual debris algorithm should be applied to short time intervals between observed arcs, less than one orbital period or at most a few orbital periods. The Keplerian integrals method, thanks to the constancy of the integrals of the two-body problem even over significant time intervals, can be used for longer time-spans, spanning several orbital periods. On the other hand, it is near to a singularity for very short time-spans and in some other near-resonance conditions, such as observations of a geosynchronous orbits at the same hour in different nights. We conclude that each method should be used in the cases in which it is most suitable as illustrated in Section 5.

3 NON-GRAVITATIONAL PERTURBATION MODEL

The solar radiation pressure represents the largest non-gravitational perturbation acting on a spacecraft in high Earth orbit. As detailed in Milani, Nobili & Farinella (1987), the solar radiation pressure mainly accounts for periodic perturbations in the eccentricity e and inclination I of the orbit. On the other hand, whenever the orbit is such that the satellite periodically enters the shadow of the Earth (as in the case of the GEO satellites), the eclipses have an important perturbative effect on the orbit, because there could be a secular effect on semimajor axis a, thus an accumulated along track displacement quadratic in time. The situation becomes worse in the case of the high A/M objects where the solar radiation pressure can become the dominant perturbative term beyond the spherical Earth approximation for A/M $\simeq 10 \, \text{m}^2 \, \text{kg}^{-1}$. Therefore, the perturbations can result in significant changes in a and/or in very large values of e and I (Valk, Lemaitre & Anselmo 2007). Moreover, for this kind of objects very little is known about their physical properties, thus preventing an effective modelling of the non-gravitational perturbations affecting them.

Other non-gravitational effects can contribute with a secular perturbation in a (see Milani & Gronchi 2010, chapter 14), including

the so-called Yarkovsky effect, which is the result of a systematic anisotropic emission of radiation, due to uneven external surface temperature, and indirect radiation pressure, due to radiation reflected and/or re-emitted by the Earth. These effects are smaller than the main component of radiation pressure in terms of the instantaneous value of the force, by a factor typically somewhere between a few parts in 1000 and a few parts in 100. Still, they can be the dominant source of perturbation in the satellite position after a number of orbital periods, while the main source of short-term perturbations remains, in almost all cases, the main anti-Sun component.

For the above reasons an adaptive non-gravitational perturbations semi-empirical model, with the following properties, was developed.

(i) For observed arcs either of total duration $\leq 0.01\,$d or with less than three tracklets, we use no non-gravitational perturbation model; thus, we solve for each set of correlated observations for only six orbital elements.

(ii) For observed arcs with at least three tracklets and total duration $>0.01\,$d, we use a model with direct radiation pressure, only the anti-Sun component, and with a free A/M parameter;[1] thus, we solve for at least seven parameters.

(iii) For observed arcs with at least four tracklets and total duration $>2\,$d, we use a model with an additional secular along track term giving quadratically accumulated along track displacement, with a free multiplicative parameter with the dimension of A/M (to ease comparison with the other term); thus, we solve for eight parameters.

The direct radiation pressure model includes a model for eclipses (with penumbra); thus, it already includes some quadratic perturbations when the orbit is subject to eclipses.

The controls used to activate the more complex models take into account not just the time-span but also the amount of observational data available in order to preserve the overdetermined nature of the least-square fit, e.g. if we were to use two tracklets in an eight-parameters fit, there would be only eight equations in eight unknown. In particular, the Keplerian integrals method of Section 2.3 has shown a good capability of finding an approximating two-body solution even for cases in which the orbit is moderately perturbed, such as a large A/M case over several days. If we were to attempt a fit with non-gravitational perturbations with the initial correlation, that is still with two tracklets, a seven-parameter orbit would be very weakly determined and instabilities of the differential corrections iterations could result in abandoning many good correlations.

Note that the semi-empirical models such as this one contain terms which are not in a one-to-one correspondence with physical effects, e.g. the along track term we have used is modelled by an acceleration in the transversal direction (orthogonal to the geocentric position and to the orbital angular momentum vectors), with an intensity proportional to the inverse square of the heliocentric distance. It may represent a Yarkovsky effect as well as secular perturbations in *a* due to radiation pressure or irregular shape (Vokrouhlický & Milani 2000). In fact, a drag term acting on a very eccentric orbit could be difficult to be discriminated (see Section 5.3).

Although the parameters are fitted, one caution is important: when using a semi-empirical parameter such as A/M, we need to constrain the values which can be determined within a physically meaningful

range. We are currently using $[-1, +200]$ as the control range for the A/M coefficient (in $\mathrm{m^2\,kg^{-1}}$) for direct radiation pressure, and $[-1, +2]$ for the one of the along track force.

4 OBSERVATIONS AND SURVEY STRATEGIES

For the purpose of this study it was decided to use existing data from observations performed at the 1-m ESASDT. The data stem from surveys and so-called follow-up observations of the year 2007. The former were optimized to search for small-size debris in the GEO region and the geostationary transfer orbit (GTO) region, with the main objective to derive statistical information. Details of the observation strategies and the survey technique are described in Schildknecht (2007). Follow-up observations, on the other hand, are used to maintain a catalogue of debris objects to allow for detailed analysis of physical characteristics, e.g. by acquiring multicolour photometry, spectra, etc. (Schildknecht et al. 2010). It is important to note that the surveys were not designed in a way to serve as a test for a 'survey only' catalogue build-up and maintenance strategy. As a consequence the resulting observations were not intended to serve as test data for orbit determination or tracklet correlation algorithms. Survey strategies optimized to build-up and maintain a catalogue of objects without the need of explicit follow-up observations are feasible, but should obviously be designed in close connection with the tracklet correlation and orbit determination algorithms.

Space debris observations at the ESASDT are organized as monthly observation campaigns consisting of about 10–14 nights centred on new Moon. Generally, there are three types of observations performed.

(i) *GEO surveys*, with a search area optimized for GEO orbits with $0°$–$20°$ inclination. The tracking during the exposure (so-called 'blind tracking') is optimized for object in GEO, thus moving the telescope 15 arcsec s^{-1} in right ascension with respect to the fixed stars.

(ii) *GTO surveys*, with a search area optimized for GTO orbits with $0°$–$20°$ inclination (Ariane GTO launches). The blind tracking during the exposure is optimized for objects in GTO, thus moving the telescope at 7.5–11.5 arcsec with respect to the stars.

(iii) *Follow-up observation* for a subset of the objects discovered in surveys (maintenance of a catalogue of debris objects). The total arcs covered by follow-up observations range from a few hours up to many months.

Table 1 gives an overview of all the ESA GEO and GTO campaigns from 2007 January until December. Note that the number of tracklets/objects given in this table does not include data from dedicated follow-up observations. The terms 'correlated' and 'uncorrelated' refer to objects/tracklets for which a corresponding

Table 1. ESA GEO and GTO campaigns.

	2007 January–December GEO/GTO
Frames	56 000
Scanned area	7600 deg^2
Total observation time	81 nights/461 h
GTO/follow-up	180 h/193 h
Correlated tracklets	483
Correlated objects	241
Uncorrelated tracklets	618

---

[1] Actually, the parameter incorporates the so-called *reflection coefficient*, which cannot be separately determined and is anyway close to 1.

catalogue object could or could not be identified, respectively. The identification procedure, or 'correlation procedure', is based on comparing the observed orbital elements and the observed position in longitude and latitude of the object at the observation epoch with the corresponding data from the catalogue. We used the unclassified part of the USSTRATCOM catalogue as our reference.

The data set for the test of the algorithms was provided by the Astronomical Institute of the University of Bern (AIUB). It contained the tracklets of all correlated and uncorrelated 'objects' from the 2007 GEO and GTO surveys, as well as the tracklets from all follow-up observations. For this, data-independent information about tracklets belonging to one and the same object, at least for the correlated objects and the objects which were followed-up intentionally, are available.

The data set contains 3177 tracklets, among them

(i) 977 uncorrelated tracklets,

(ii) 747 correlated tracklets of 349 correlated objects ('correlated' = correlated with USSTRATCOM TLE catalogue),

(iii) 1453 tracklets from intentional follow-up observations of 240 objects.

The uncorrelated and the correlated tracklets were found in the GEO and GTO surveys, but also during follow-up observations instead or in addition to tracklets of objects to be followed up. The surveys covered the GEO region rather homogeneously but were not optimized to re-observe objects, e.g., from night to night. Based on results by Jehn et al. (2006) and Schildknecht et al. (2008), these 977 uncorrelated tracklets could belong to 300–500 objects.

The tracklets of the objects which were intentionally followed up have very particular characteristics, which are non-typical for survey observations and thus worth mentioning. These objects belong to an AIUB-internal catalogue of small-size debris in GEO- or GTO-like orbits. The catalogue is biased towards objects with high A/M due to deliberate selection. For a newly detected object, the standard procedure consists of acquiring one to four follow-up observations during the night of discovery, resulting in arcs of 0.5–5 h. Additional one to two follow-up observations are then performed during the nights following the discovery, eventually followed by regular observations every month. It is, again, worth noting that the temporal distribution of these follow-up observations does not at all represent typical space debris survey or surveillance (SSA) scenarios.

The available arc length for the majority of the objects which were followed-up during the 2007 campaigns is less than one day (see Fig. 2). For 46 objects, however, an arc length of more than 57 d is available.

The tracklet data were provided in the form of so-called 'tracklet files' of the Pan-STARRS Data Exchange Format (DES). The DES is described by a complex document, which introduces the necessary concepts, fixes one standard terminology, defines the data types with an object-oriented style, assigns formats and procedures for exporting/importing all the data types.

In these files, observations pertaining to the same tracklet are identified by a unique 'tracklet identifier'. The assignment of individual observations to a tracklet is (by definition) done by the 'observer' as it is intimately related with the survey and the object-detection algorithms. A typical survey will, though, not provide any information about 'objects', i.e. about the mutual correlation of tracklets. However, if such information is available, it may be coded in the so-called 'secret names'. This information (discriminating between uncorrelated tracklets, correlated objects or follow-up ob-
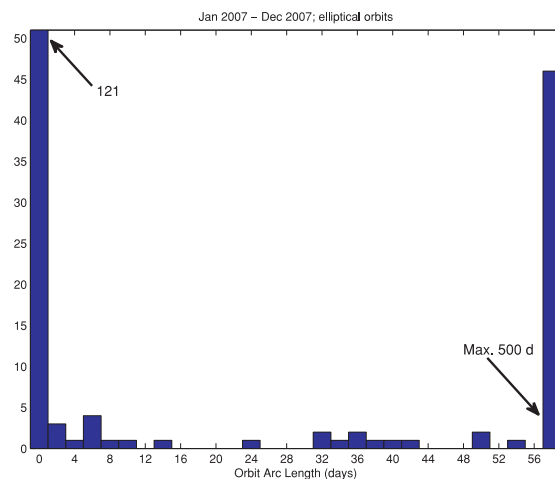
Figure 2. Histogram of the arc length for the objects which were intentionally followed-up during the 2007 campaigns.

servation of correlated objects) is not to be used in the test phase, but it is stored in order to allow a final comparison with the 'ground truth'.

5 RESULTS FROM A 1-YEAR EXPERIMENT

The new algorithms and the related software described in Section 2 were applied to the data set described in the previous section. The purpose was to show that these algorithms are adequate for a future catalogue build-up activity by ESA, e.g. in the context of the SSA initiative. Thus, we selected a time interval long enough that we can presume a future SSA survey would have observed all target objects within such a period, and short enough to allow for accurate orbit determinations with our semi-empirical non-gravitational perturbations model. We selected the lunation as a kind of natural time unit for observations. The tracklets of objects observed several times within one lunation should be correlated. On the contrary, objects observed only once per lunation may not be correlated, because this is well beyond the SSA specifications.

5.1 The test on 1 year of data

As explained in Section 4, the data set contained three classes of tracklets: the ones correlated by attribution to TLE objects, the ones correlated by AIUB (in most cases, by targeted follow-up) and the ones for which no correlation was previously known.

The data base of tracklets was split in 12 lunations. The algorithms described in Section 2 were applied to each lunation separately. The correlations within each lunation are normalized, thus there are no duplicates, using the correlation management procedure (see Section 2.4).

Out of 3177 input tracklets, 1503 were correlated, 1674 left uncorrelated. Of course we have no way to know how many should have been correlated, that is how many physically distinct objects are there: in particular, objects re-observed at intervals longer than 10 d have escaped correlation, because we did not try to perform the first step when the time-span between two tracklets exceeds 10 d. As already pointed out in Section 4, the observations were not scheduled to allow for orbit determination of all the objects, but only for some of them, in particular the uncorrelated objects which were of interest as candidate high A/M cases.

5.2 The global orbit catalogue

Joining the orbits computed in each lunation, we obtained 202 correlations with a good orbit and more than two tracklets. This process might generate duplications of orbits for the same object. In fact, if two orbits for the same object are computed in different lunations, it is not always possible to correlate them, especially if the two lunations are not consecutive. We plan to investigate the issue of duplications in this catalogue in the future.

Figs 3–6 show the distribution of the computed orbits in terms of orbital elements and absolute magnitude.

The orbits in the (a, e) plane (Fig. 3) show a concentration of objects with semimajor axis close the geostationary radius, including some with high eccentricity. Some of these latter objects have a high value of the A/M parameter, as described in Section 1. In the upper left corner the objects in GTO can be found with $e \simeq 0.7$. Fig. 4 shows the same orbits in the (I, e) plane.
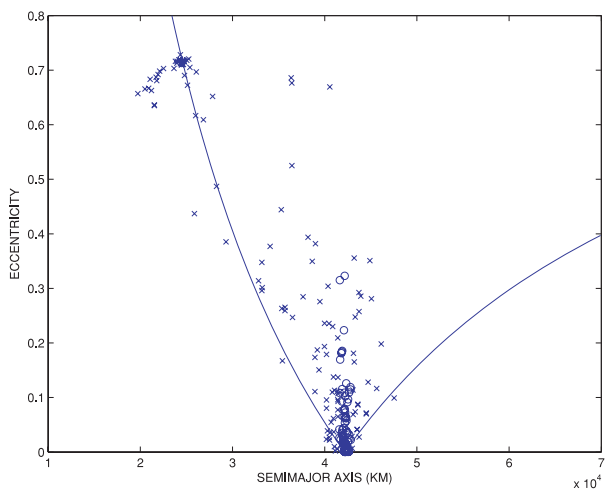

Figure 3. Distribution in semimajor axis versus eccentricity of the computed orbits. The circles indicate objects with semimajor axis between 41 464 and 42 864 km, i.e. nearly geostationary. The crosses indicate all the other orbits. The lines bound orbits crossing the GEO radius at apogee (left curve) or at perigee (right curve).
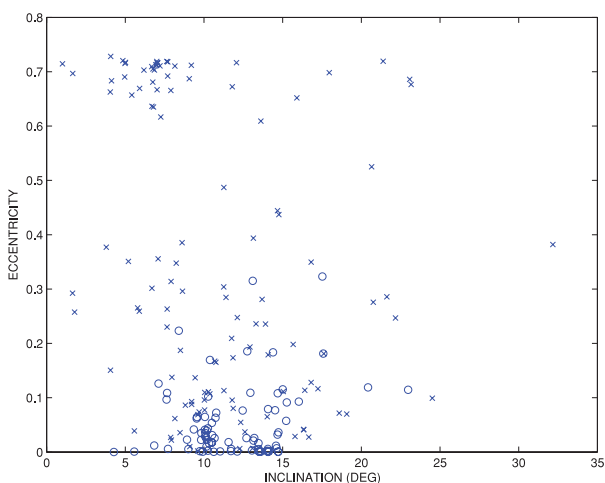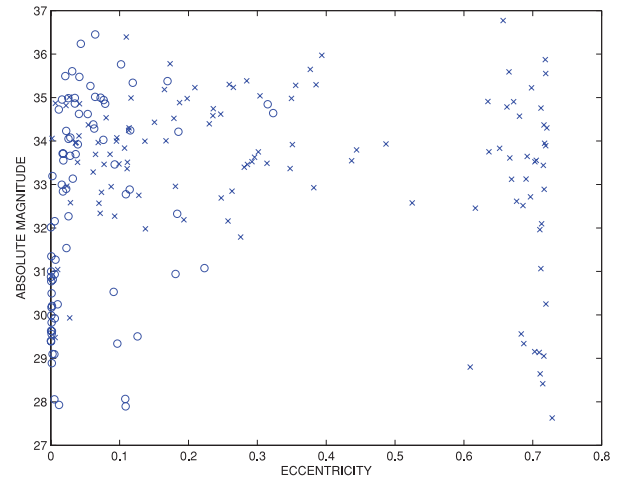

Figure 4. Distribution in inclination versus eccentricity of the computed orbits. The circles indicate objects with semimajor axis between 41 464 and 42 864 km, i.e. nearly geostationary. The crosses indicate all the other orbits.

Figure 5. Distribution in eccentricity versus absolute magnitude of the computed orbits. The circles indicate objects with semimajor axis between 41 464 and 42 864 km, i.e. nearly geostationary. The crosses indicate all the other orbits.
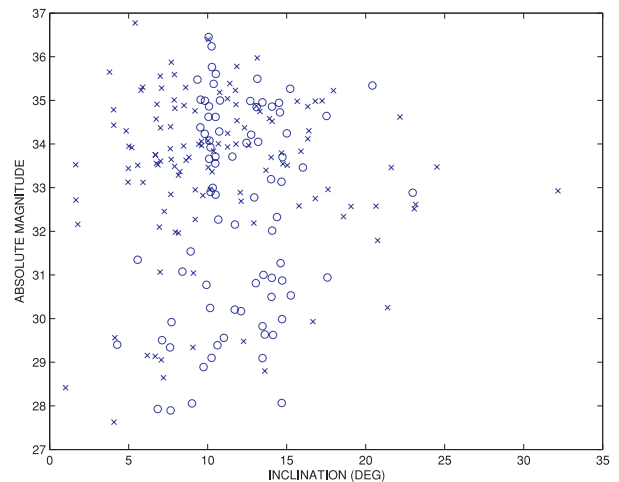

Figure 6. Distribution in inclination versus absolute magnitude of the computed orbits. The circles indicate objects with semimajor axis between 41 464 and 42 864 km, i.e. nearly geostationary. The crosses indicate all the other orbits.

Fig. 4 shows an apparent lack of really GEOs, with low e and I: actually there is only one orbit with $e < 0.01$ and $I < 5°$. This is due to the fact that the survey conducted by the ESASDT in 2007 had the purpose of discovering new objects, and the geostationary objects are mostly active satellites, whose orbits and ephemerides are known. Thus, the fields of view were on purpose avoiding the *geostationary line*, the line on the celestial sphere corresponding to the exactly geostationary satellites (with $e = 0, I = 0°$).

Figs 5 and 6 show the distribution of eccentricity/inclination versus intrinsic luminosity of the objects, the latter described in the absolute magnitude scale. The absolute magnitude H is computed by least-squares fit of the photometry data to the computed apparent magnitudes h, according to the rule

$$h = H - 5\log_{10}(d) - 5\log_{10}(d_\odot) - F(\phi, G), \qquad (6)$$

where d is the distance (in au) from the observer to the object, $d_\odot$ the distance from the object to the Sun (practically 1 au), ϕ the phase,

G a *slope parameter* which depends upon the optical properties of the object surface, especially albedo, and *F* a function for which we have an International Astronomical Union (IAU) standard formula (Bowell et al. 1989, equation A1) devised for asteroids. The value of *G* is assumed by default to be 0.15, and is redetermined by fitting to the results of dedicated photometric studies for individual asteroids. There is essentially no information on the value of *G* for debris, not even on the applicability of the IAU formula for $F(\phi, G)$. To solve for *H* we have assumed $G = 0.15$, which is just a first guess, that is, formula (6), with $G = 0.15$, is used as a definition of a conventional value of the absolute magnitude *H*.

Whatever the exact definition, it is not easy to convert an absolute magnitude into a size, because of the wide range of albedo values, the poor knowledge of the phase effects, and also because of irregular shapes and inhomogeneous surface coating. However, if we could assume albedo 0.1 and a spherical shape, by the relationship between *H* and size which is consequence of the IAU standard formula (Bowell et al. 1989, equation A6) devised for asteroids, we would get an absolute magnitude *H*, for an object in Earth orbit of diameter *d* in meters, as follows:

$$H = 33.1 - 5 \log_{10}(d).$$

From this formula we get a diameter ranging between $\simeq$30 and 10 m for the correlated objects. Thus, the largest objects should be satellites (at low *e*) and rocket stages (near GTO), the smallest are certainly fragmentation debris or mission-related objects.

The existence of objects with high *e* and also *I* was already well known, what is interesting is that some of these have a quite large cross-section. Understanding the dynamics of such objects is a challenge, which requires advanced models and a good data set of both astrometry and photometry.

5.3 Determination of non-gravitational parameters

As previously pointed out in Section 3, it is important to succeed in determining the perturbations due to non-gravitational effects. The algorithms were modified in order to handle this task. This implies not just to have a non-gravitational perturbation model in the orbit propagator, but also to apply the adaptive model progressively as the correlations build up, with the semi-empirical parameters gradually added to the list of variables to be solved.

In Figs 7 and 8, the distributions of the values of non-gravitational parameters computed for a subsample of the objects displayed in Fig. 3 are shown. In particular, it was possible to compute the A/M parameter for 142 objects. For 59 objects also the along track perturbation (called ATP parameter) was determined. Note that we cannot discriminate between a true Yarkovsky effect (due to thermal emission) and an effect of direct radiation pressure on a complex shape debris, or even from a different type of drag-like force, as discussed in Section 3.

Whereas the bulk of the objects lies in the first histogram bin, a significant fraction of them belong to the so-called large A/M population. 69 per cent of the computed A/M parameters are significant (value >2 rms); these include the extreme case of an estimated value $142 \pm 24 \, \mathrm{m^2 \, kg^{-1}}$. For the ATP, 56 per cent of the computed parameters are significant (value >2 rms); however, the largest positive value is $0.84 \pm 0.59 \, \mathrm{m^2 \, kg^{-1}}$ and is not significant. The two largest negative ATP values are well determined (-0.329 ± 0.001 and $-0.311 \pm 0.002 \, \mathrm{m^2 \, kg^{-1}}$) but correspond to GTO; thus, the drag-like effect is to be interpreted as a true drag occurring near perigee, which cannot be discriminated from a nearly constant transversal negative acceleration because observations are obtained only near
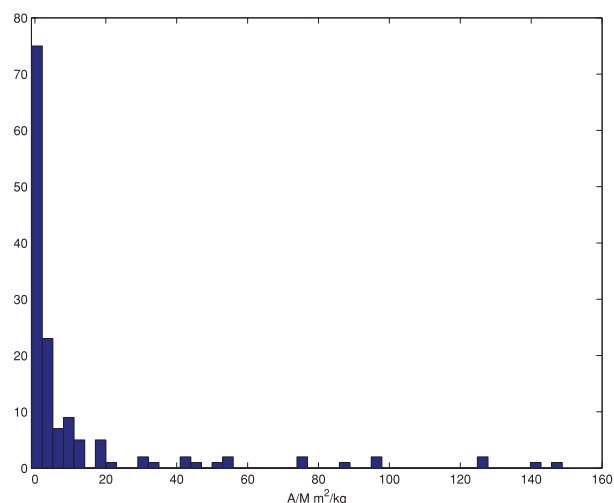

Figure 7. Distribution of A/M parameter for the 142 objects with enough observations to allow for this determination.
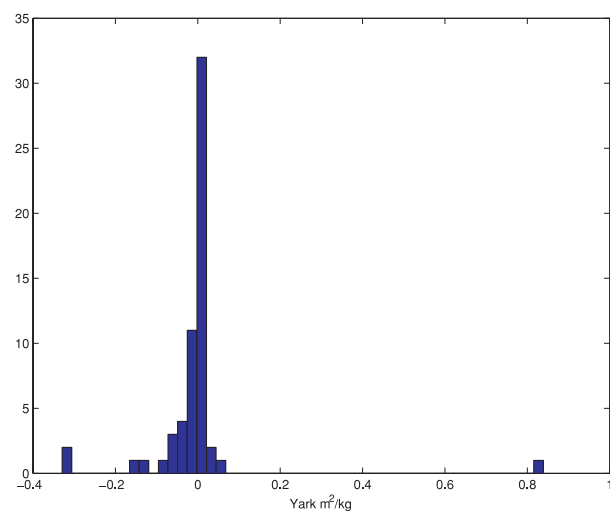

Figure 8. Distribution of the ATP for the 59 objects with enough observations to allow for this determination.

apogee. In conclusion, the secular along track acceleration due to radiation effect, both direct and thermal, can be detected by the orbit determination process but has ATP values typically below $0.1 \, \mathrm{m^2 \, kg^{-1}}$ in absolute value.

The problem is that we did not have any 'ground truth' to compare our results on non-gravitational perturbations; for this we would need to have a catalogue with orbits and non-gravitational parameters from other sources. On the other hand, the objects on which to perform such a comparison should be carefully selected, among those with the best determination not just of the orbit but also of the semi-empirical parameters. These 'good cases' might require fitting more than one month of data, with a large enhancement of the ATP effect. This problem will need to be further investigated.

5.4 Assessment of the results

Once a catalogue of orbit is obtained, it would be important to be able to judge the performance of the algorithms and the reliability of the catalogue itself. In the present analysis, no absolute 'ground

Table 2. Summary of the comparison with AIUB for the first lunation. Between parentheses we highlight the number of occurrences where we identified the reason for the smaller or missed correlations with an observation strategy not optimized for our algorithms. See text for details.

Number of tracklets	Equal	Larger	New	Smaller	Missed	Mixed
16	–	–	–	–	–	1
10–11	1	–	–	1	–	–
7–8	7	1	1	–	–	–
4–6	7	3	–	1	1 (1)	–
3	4	3	2	3 (3)	1 (1)	–

Table 3. Summary of the comparison with AIUB for the second lunation. Between parentheses we highlight the number of occurrences where we identified the reason for the smaller or missed correlations with an observation strategy not optimized for our algorithms. See text for details.

Number of tracklets	Equal	Larger	New	Smaller	Missed	Mixed
11–12	–	3	–	–	–	1
7–9	3	–	–	3 (1)	–	1
4–6	12	5	–	8 (4)	7 (6)	–
3	10	1	3	3 (2)	6 (4)	1

truth' (that is an orbit catalogue used as input for the data simulation) was available to validate the catalogue. None the less, a meaningful comparison, giving an indication of the validity of the procedure, was possible by comparing with the correlation results obtained by the group that produced the data set itself. This implies that it is not always possible, in case of a discrepancy between the two catalogues, to decide 'who is right'. Fortunately, this was not necessary. The goal was to show that the new algorithms allow us to obtain substantially the same results obtained by the AIUB group, without having access to the scheduling information. Namely, if an uncorrelated object has been the target of deliberate follow-up, the AIUB group had the correlation information a priori (and the same information could be obtained for a correlated object, just by comparing with the ephemerides). On the other hand, the present analysis did not use any a priori information.

To make an in-depth study, we selected the two lunations which included the largest number of tracklets, namely the first and the second one. In Tables 2 and 3, we show a summary of the results obtained.

The meaning of the table columns is the following:

(i) *equal* indicates the cases in which the new algorithms obtained the same correlation reported by AIUB;

(ii) *larger* indicates the cases in which the new algorithms added some additional tracklets to those considered by AIUB in their correlation;

(iii) *new* indicates correlations not found by AIUB, i.e. orbits computed by the new algorithms using just non-correlated tracklets;

(iv) *smaller* indicates the cases in which the new algorithms got a correlation using a subset of the tracklets used by AIUB;

(v) *missed* indicates the cases in which the new algorithms did not get the correlation reported by AIUB;

(vi) *mixed* indicates the cases in which the new algorithms obtained a correlation using a partly different set of tracklets with respect to AIUB, that is the new algorithms got a correlation using

some (but not all) of the tracklets exploited by AIUB and, at the same time, added some non-correlated tracklets.

A deeper analysis of the underlying reasons for the smaller and missed correlations shows that some of them could be traced back to the observation strategy. As pointed out several times, the observation strategy adopted by AIUB to obtain the data used in this study was not intended for the exploitation of the algorithms described in Section 2. In particular, the requirement of avoiding the singularities described in Section 2.3 was not considered, because the very existence of such a problem was not known at the time.

As already discussed, the two algorithms have a limiting time-span (different for the two methods) between consecutive tracklets above which a correlation is unlikely to be found. An observation strategy optimized for the use of these algorithms should take into account this requirement, but for the same reason above, this was not the case for the AIUB data used in this study. The cases in which we were able to attribute the smaller or missed correlations to the observational strategy are highlighted in the tables with the number written between parentheses: these cases include both the observations at the same hour in the night and the observations separated by a time interval exceeding 5–6 d.

The cases of two-tracklet correlations were deemed not reliable. As a matter of fact, the typical rms in the semimajor axis for this orbits were thousands of km for observations taken in the same night. Therefore, the probability of being true if a longer time-span was available is judged to be very low. A comparison among the two-tracklet correlations proposed by AIUB and the new method shows a very large fraction of disagreement. The indication is that two-tracklet correlations are to be considered as an intermediate data product, not a result, that is they are accepted only if and when it is possible to confirm them with the correlation of a third tracklet.

The results just discussed show a good agreement to the ones obtained by AIUB. The number of cases of 'superior' results (columns *larger* and *new*) compensates the 'inferior' results (columns *smaller* and *lost*), especially if the cases in which the observing strategy was unsuitable are discounted.

Thus, we showed that it is possible to build up a catalogue from scratch, without any prior correlation information. This *catalogue build-up* phase is necessarily the first phase of a new programme such as SSA, because correlation information is not available, or available only for a comparatively small subset of the target population of the new survey.

Moreover, we showed that the presence of non-gravitational perturbations, whose parameters are not known a priori and can be quite large, does not increase the difficulty of the initial catalogue build-up. The determination of some non-gravitational perturbation parameters can be done simultaneously with the correlation and orbit determination procedure. To achieve this goal a suitable observing strategy should be used: in particular for the geosynchronous belt one tracklet per night is enough, but 'equal hour' singularities and time intervals, between tracklets of a given object, significantly larger than one day should be avoided.

Of course, to obtain the result of building up a large catalogue of satellites and space debris, down to sizes smaller than the ones for which orbits are now available, the mobilization of appropriate resources is required. These include sensors more powerful than the current experimental ESASDT (in particular with a larger field of view), and adequate software, such as a scheduler with the capability of taking into account the requirements from orbit determination, and a fully tested correlation and orbit

determination software which could be based upon the demonstration software we have developed.

6 CONCLUSIONS

As stated by ESA, 'the European Space Situational Awareness (SSA) Programme serves the strategic aims of the European Space Policy (ESP) by supporting the independent capacity to securely, sustainably and safely operate Europe's critical space infrastructure'.

In the next few years, the SSA initiative will enter its definition and practical implementation phase. One of the goals of the SSA programme is to provide a European catalogue of Earth-orbiting objects similar to the American TLE catalogue. This goal requires the realization of a space surveillance network of radar and optical sensors capable of detecting and tracking a large number of objects.

Whereas the definition of the network is still in progress, it is clear that the availability of efficient methods for orbit determination is of paramount importance in improving the efficiency of the network. It is worth stressing that an efficient and computationally intensive orbit determination procedure can act in a twofold way in the definition of the network. From one side, given a certain network design, it allows us to reach more ambitious goals in terms of cataloguing performances, e.g. allowing the cataloguing of objects with lower diameter limit or the cataloguing of more elusive objects such as the high A/M objects. It must be noted at this stage that the size limit within the TLE catalogue is dictated not only by sensor limitations, but also by limits in the handling and computer processing of the observational data. On the other side, given the preliminary requirements of a surveillance network (e.g. in terms of the minimum size of the objects to be catalogued), the adoption of an efficient orbit determination method allows significant savings in the design of the sensors.

In this paper it was shown how the methods described in Section 2 allowed the determination of six-parameters orbits from a standard data set of optical observations. No a priori information nor simplified assumptions (such as circular orbits) were required, and the observation strategy was completely independent from the design of the methods and not optimized for their use. Even the most demanding cases of high A/M objects were successfully treated.

The results of this study clearly show that the methods described in Section 2 can represent an important tool in the SSA data processing. In Farnocchia et al. (2010), an extension of the Keplerian integrals method, including the J_2 perturbation, was presented, thus allowing the correct treatment of objects in LEO. The application of the method to LEO optical data will be presented in a paper in preparation.

ACKNOWLEDGMENTS

REFERENCES

Bowell E., Hapke B., Domingue D., Lumme K., Peltoniemi J., Harris A. W., 1989, in Binzel R. P., Gehrels T., Shapley Matthews M., eds, Proc. Conf. Asteroids II. Univ. Arizona Press, Tucson, p. 524

Choc R., Jehn R., 2010, Classification of Geosynchronous Objects. ESA Space Debris Office, Darmstadt

Farnocchia G., Tommei G., Milani A., Rossi A., 2010, Celest. Mech. Dynamical Astron., 107, 169

Gronchi G. F., Dimare L., Milani A., 2010, Celest. Mech. Dynamical Astron., 107, 299

Jehn R., Ariafar S., Schildknecht T., Musci R., Oswald M., 2006, Acta Astronaut., 59, 84

Liou J.-C., Weaver J. K., 2005, in Danesy D., ed., ESA SP-587, Proc. 4th European Conf. Space Debris. ESA, Noordwijk, p. 285

Maruskin J. M., Scheeres D. J., Alfriend K. T., 2009, J. Guidance Control Dynamics, 32, 194

Milani A., 1999, Icarus, 137, 269

Milani A., Gronchi G., 2010, Theory of Orbit Determination. Cambridge Univ. Press, Cambridge

Milani A., Nobili A., Farinella P., 1987, Non-gravitational Perturbations and Satellite Geodesy. Adam Hilger Ltd., Bristol, UK

Milani A., Sansaturio M., Chesley S. R., 2001, Icarus, 151, 150

Milani A., Gronchi G. F., de' Michieli Vitturi M., Knežević Z., 2004, Celest. Mech. Dynamical Astron., 90, 59

Milani A., Gronchi G. F., Knežević Z., Sansaturio M. E., Arratia O., 2005, Icarus, 79, 350

Milani A., Gronchi G. F., Farnocchia D., Tommei G., Dimare L., 2009, in Lacoste H., ed., SP-672, ESA Proc. Fifth European Conf. Space Debris. ESA, Noordwijk (CD-Rom)

Musci R., Schildknecht T., Ploner M., 2010, Acta Astron., 66, 693

Rossi A., 2011, Scholarpedia, 6, 10595

Schildknecht T., 2007, A&AR, 14, 41

Schildknecht T., Musci R., Ploner M., Beutler G., Flury W., Kuusela J., de Leon Cruz J., de Fatima Dominguez Palmero L., 2004, Advances Space Res., 34, 901

Schildknecht T., Musci R., Flury W., Kuusela J., de Leon J., de Fatima Dominguez Palmero L., 2005, in Danesy D., ed., ESA SP-587, Proc. 4th European Conf. Space Debris. ESA, Noordwijk, p. 113

Schildknecht T., Flohrer T., Musci R., Jehn R., 2008, Acta Astron., 63, 119

Schildknecht T., Früh C., Herzog A., Hinze J., Vananti A., 2010, Proc. 2010 AMOS Tech. Conf., http://www.amostech.com/TechnicalPapers/2010.cfm

Tommei G., Milani A., Rossi A., 2007, Celest. Mech. Dynamical Astron., 97, 289

Tommei G., Milani A., Farnocchia D., Rossi A., 2009, in Lacoste H., ed., ESA SP-672, Proc. Fifth European Conf. Space Debris. ESA, Noordwijk (CD-Rom)

Valk S., Lemaitre A., Anselmo L., 2007, Advances Space Res., 41, 1077

Vokrouhlický D., Milani A., 2000, A&A, 362, 746

This paper has been typeset from a TEX/LATEX file prepared by the author.